ACS OMEGA

http://pubs.acs.org/journal/acsodf

Article

Improved Adsorption of Tetracycline in Water by a Modified *Caulis spatholobi* Residue Biochar

Zheng Fan,* Jie Fang, Guoliang Zhang, Lei Qin, Zhenzhen Fang, and Laiyun Jin

Cite This: *ACS Omega* 2022, 7, 30543−30553

Read Online

ACCESS | Metrics & More | Article Recommendations

ABSTRACT: A potassium modified biochar (KBC) using *Caulis spatholobi* residue as the raw material was prepared by adopting a two-step method of pyrolysis followed by high-temperature potassium hydroxide activation, and its properties were characterized. Activation using potassium hydroxide under high temperature induced the loss of $CaCO_3$ and partial C on biochar, which created a high specific surface area (1336.31 m^2/g) together with a developed pore structure. pH displayed a slight influence on tetracycline adsorption, which signified the slight influence of the existence of tetracycline and the charge potential of biochar. Besides, pore filling, hydrogen bonding and $\pi-\pi$ EDA stacking interactions possibly resulted in tetracycline adsorption on biochar. Tetracycline adsorption was fast in the original period, followed by a slower rate of adsorption until equilibrium was reached. Adsorption kinetics of tetracycline could be described using secondary and Elovich kinetic models. Adsorption isotherms for tetracycline were well fitted to the Langmuir isotherm model, and the maximum adsorption capacity of KBC was 830.78 mg/g at 318 K. According to a study of the thermodynamics, the adsorption of tetracycline on KBC was an endothermic reaction process. Corresponding results in the present study demonstrated that high-temperature potassium hydroxide activation enabled biochar to effectively eliminate tetracycline from water and wastewater.

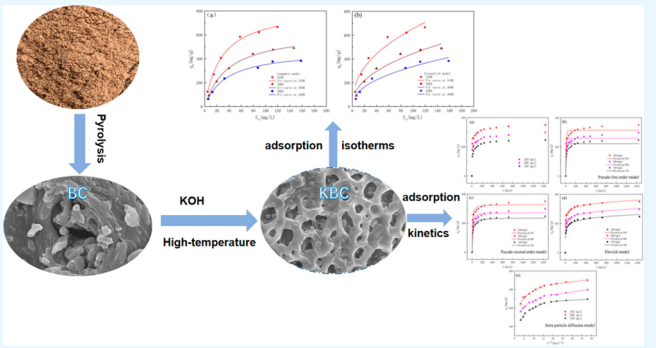

1. INTRODUCTION

Since penicillin was discovered in 1928, the application of antibiotics has risen sharply.[1] However, this sharp rise in use has caused the unintentional release of antibiotics into the environment, a potential source of ecological problems. Trace quantities of veterinary and human antibiotics have recently been identified in various matrices,[2−4] especially in the aquatic environment.[5] Tetracycline (TC) is one of the most extensively applied antibiotics globally, primarily in the treatment of animal diseases and in animal husbandry.[6] TC can be released into the aquatic environment in both its primary and metabolic forms,[6] and TC pollutants can adversely affect the entire ecosystem, not only spawning highly resistant strains of bacteria[7] but also seriously harming aquatic life forms.[8] In addition, these pollutants can threaten human health by means of drinking water and the food chain.

There are many approaches to TC removal in current use, including biological treatment,[9] oxidation techniques,[10] adsorption,[11] membrane osmosis,[12] and ultrasonic cavitation.[13] Adsorption is one of the most normally employed approaches based on the ease of use, low cost, high efficiency, as well as absence of secondary pollution. Biochar—a carbon-rich solid that can be acquired through heating biomass in an oxygen-deficient environment—possesses a porous structure similar to that of activated carbon and, as such, is one of the most frequently applied and efficient adsorbents for use in eliminating a range of pollutants from water.[14−16] Biochar features are a porous structure, high specific surface area, rich surface functional group structure, and high mineral content. It has proven effective in removing TC from wastewater and is therefore often used in the treatment of antibiotic wastewater.[17] Various types of biomass are used to make biochar, with agricultural and forestry biomass—one of the most abundant renewable resources on Earth[18]—such as bamboo, straw, and fruit shell[19−21] being the primary source.

Waste products from Chinese herbal medicine are abundant in China.[22,23] Thus, it is both economical and environmentally friendly to use such waste products as raw materials to prepare biochar. However, the adsorption capacity of biochar prepared by direct high-temperature cracking is generally low, which could be ascribed to limited pore structures, specific surface area, and mere functional groups on biochar with high charring

Received: June 28, 2022
Accepted: August 10, 2022
Published: August 19, 2022

© 2022 The Authors. Published by American Chemical Society

https://doi.org/10.1021/acsomega.2c04033
ACS Omega 2022, 7, 30543−30553

temperature. Thus, an activator is needed to improve pore structures and specific surface areas of biochar, consequently reaching a higher adsorption capacity.[24] For instance, de-ashing treatment using HCl/HF enabled sludge-derived biochar was used to create an extremely high specific surface area together with a developed pore structure, which behaved excellently on adsorbing organic pollutants.[25] *Caulis spatholobi* is used in herbal medicine due to its various pharmacological effects, such as improving the hematopoietic system, regulating immunity, and antitumor, antivirus, and antioxidation properties.[26] It is rich in lignin, cellulose, hemicellulose, polysaccharides, phenolic ketones, and other macromolecular compounds that contain hydroxyl, amino, ether, and other functional groups.

The present study aimed to prepare high-performance biochar for removing TC. Activation using potassium hydroxide (KOH) under high temperatures was used to prepare biochar with a developed pore structure and specific surface area. The effect of biochar dosages and pH on TC adsorption, as well as the adsorption kinetics, thermodynamic properties, and adsorption capacity for TC, were studied.

2. MATERIALS AND METHODS

2.1. Materials and Reagents. *Caulis spatholobi* ("chicken blood vine") residue (BR) applied in the current work was acquired from a pharmaceutical company in Hangzhou, Zhejiang Province. Sodium hydroxide (NaOH, AR) and hydrochloric acid (HCl, 37%, AR) were acquired from Xilong Science Co., Ltd., and potassium hydroxide (KOH, AR) was from the Sinopharm Chemical Reagent Co.

2.2. Preparation of the Biochar. The collected dregs of *Caulis spatholobi* were cleaned with deionized water and dried in an oven at 60 °C. Besides, the dried samples were then crushed and sieved using a 0.18 mm sieve with the purpose of obtaining a uniform fine powder for use as a raw material.

2.2.1. Preparation of BC. The raw material was transferred to a quartz boat, which was subsequently positioned in the center of a tube furnace and heated up to 900 °C at 5 °C/min based on a nitrogen atmosphere. Besides, the sample was pyrolyzed for 2 h and then permitted to cool naturally to ambient temperature. Then, the sample was removed and rinsed with 1 M hydrochloric acid to remove impurities, followed by rinsing with deionized water to remove residual chemical reagents on the biochar, and subsequently dried in the oven at 80 °C for 12 h with the purpose of obtaining the product labeled "BC". The yield of biochar was 35.4%.

2.2.2. Preparation of KBC. The BC obtained above was mixed with KOH to produce three mixtures with diverse mass ratios (KOH/BC = 1:1, 2:1, 3:1), which were then transferred to a mortar and pestle and ground thoroughly to ensure that the two were thoroughly intermixed. The ground mixture was then transferred to a quartz boat and subjected to the same heating and chemical treatment as the BC. The final product was labeled as "KBC". A yield of 27.4% could be obtained on KBC, lower than that for BC. Activation using KOH and HCl can remove minerals in biochar, thus resulting in the decline in the yield of activated biochar.

2.3. Characterization. With parameters of 15 s equilibration intervals, 1.00 g/cm^3 sample density, and 15.0 cm^3/g low pressure dose, the Brunauer, Emmett, and Teller (BET) test was adopted for determining the specific surface area and pore volume of the adsorbents (ASAP 2020 PLUS, MICROMERITICS, USA). Then, the surface functional groups were identified using Fourier transform infrared spectroscopy (FTIR) and a Nicolet 6700 spectrometer (Thermo Nicolet, USA) in wavenumbers within the range from 500 to 4000 cm^{-1}. The surface morphology of the samples was studied based on scanning electron microscopy (SEM) (SU8010, Hitachi, Japan) in 10 kV of acceleration voltage. Besides, X-ray diffraction (XRD, X'PertPRO, PNAlyptal, The Netherlands) in a 2θ range of 10−80° was used to study the crystallinity of the samples at 40 kV of working voltage and 40 mA of working current. In addition, the zero-point charge (pHpzc) of the modified biochar surface was determined using a Nano ZS90 nanoparticle sizer (Zeta potential, Malvern, UK), and the absorbance of TC was measured using a Shimadzu 1800 UV−vis spectrophotometer (Japan). The maximum wavelength of TC obtained by scanning was 353 nm.

2.4. Batch Adsorption Experiments. The impact of the quantity of adsorbent on the degree of TC adsorption was studied using a range of concentrations of BC and KBC (0.25, 0.5, 0.75, 1.0, and 1.25 g/L). The impact of pH on TC adsorption was also explored through controlling the pH in the range 1−10 using 1 M NaOH and 1 M HCl solutions. In all experiments, a certain amount of adsorbent was supplemented in a 100 mL beaker including 50 mL of a given concentration of simulated TC wastewater solution; this beaker was then covered to protect the contents from light and stirred using a magnetic stirrer for a day before the sample was then filtered using a 0.45 μm filter membrane.

Measurement of the adsorption kinetics was performed at 298 K, which was controlled by a water bath. The adsorbent dose was 0.5 g/L supplemented to three different concentrations of simulated TC contaminated wastewater solution (150, 200, 250 mg/L). These solutions were sampled at various time intervals from 10 to 1440 min following mixing. Adsorption equilibrium experiments were made at 298, 303, 308, and 318 K with solutions with initial TC concentrations within the range from 150 to 400 mg/L. Both adsorbent dose and pH values were kept constant in these experiments. In terms of all of the samples, the absorbance of TC was calculated based on the adsorption at 253 nm by a UV−vis spectrophotometer and a previously constructed TC calibration curve. Moreover, we repeated all of the experiments three times. Besides, the results were averaged. Then, the adsorption capacity (q_e) and the removal precent of TC (R, %) were computed based on eqs 1 and 2, separately:[27]

$$q_e = \frac{C_0 - C_t}{W} V \tag{1}$$

$$R, \% = \frac{C_0 - C_t}{C_0} 100\% \tag{2}$$

where C_0 refers to the initial concentration, C_t is the concentration at time t, W is the mass of the adsorbent, and V is the volume of solution.

2.5. Assay of Desorption and Regeneration. As illustrated in a previous study, sodium hydroxide (NaOH) could desorb residual TC on biochar.[28] In the present study, 0.1 M NaOH was mixed with biochar at 20 °C for 24 h. Repeated desorption using NaOH was conducted until the desorbed NaOH solution became colorless. The amount of TC in desorbed NaOH was analyzed. Afterward, deionized water was used to clean biochar upon desorption process, until the pH of washing water remained unchanged. Next, we dried the washed biochar at 80 °C to obtain the regenerated

https://doi.org/10.1021/acsomega.2c04033
ACS Omega 2022, 7, 30543−30553

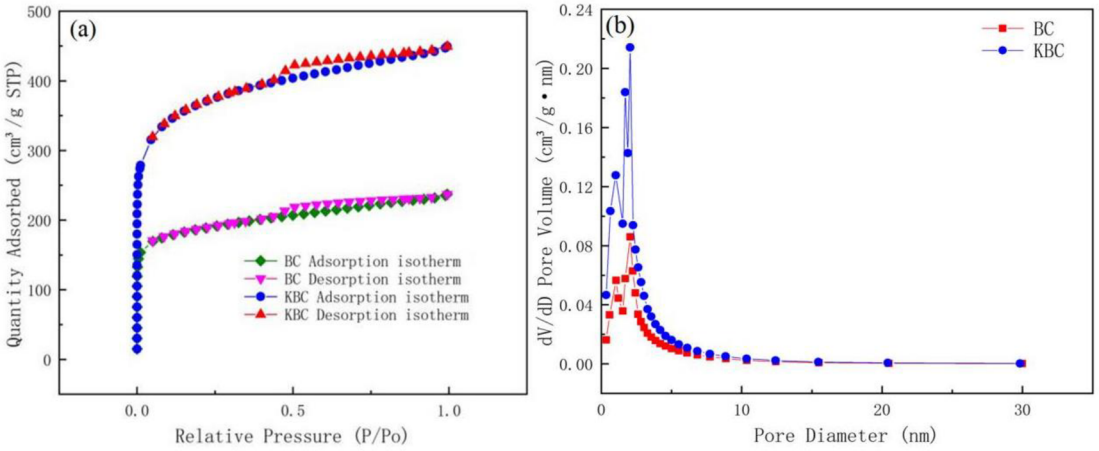

Figure 1. N_2 adsorption/desorption isotherms (a) and pore size distribution (b) for the BC and KBC adsorbents.

adsorbent. By performing four cycles of adsorption and desorption, the efficiency of regeneration was determined.

3. RESULTS AND DISCUSSION

3.1. Characterization of the Adsorbent. *3.1.1. N_2 Adsorption/Desorption Isotherm and Pore Properties.* With the aim of high-temperature KOH activation, the greatest specific surface area and most developed pore structures should be detected on KBC, rather than BC and raw BR.

Table 1. Determinations of the Specific Surface Area and Pore Structure of BC and KBC

sample	S_{BET} (m^2/g)	$S_{Langmuir}$ (m^2/g)	S_{Micro} (m^2/g)	V_{Total} (cm^3/g)	V_{Micro} (cm^3/g)
BC	694.35	992.41	511.25	0.367	0.209
KBC	1336.31	1882.36	986.03	0.695	0.409

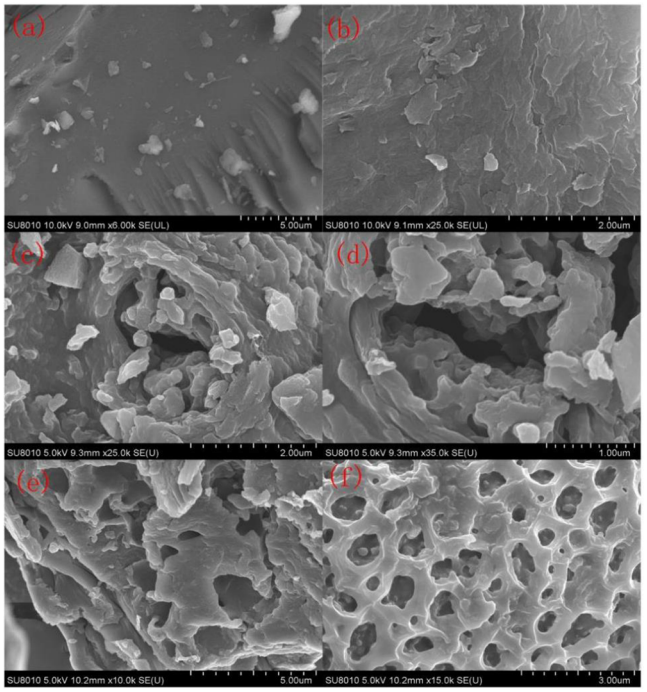

Figure 2. SEM images of the raw BR (a, b), pyrolyzed BC (c, d), and modified pyrolyzed KBC (e, f).

Table 2. EDS Elemental Analysis of the BR, BC, and KBC Samples

element (wt %)	BR	BC	KBC
C	53.29	86.68	82.91
N	2.58	1.54	1.58
O	40.76	7.42	8.84
Al	0.06	0.08	0.16
Ca	2.98	3.96	3.03
K	0.34	0.32	3.48

Figure 1a presents the N_2 adsorption/desorption isotherms of the BC and KBC adsorbents. Both BC and KBC exhibit both type I and type IV isotherms, corresponding to microporous and mesoporous structures on biochar.[29] The rapid increase in adsorbed N_2 at very low P/P_0 is indicative of the existence of microporous structures in the two adsorbents, while the poor overlap of the N_2 adsorption/desorption curves at higher P/P_0 values shows that the pore inner surface area of both biochars was much larger when compared with the pore outer surface area, a sign pointing to the existence of mesoporous structures as well as micropores.[30] The pore size distributions within BC and KBC were obtained by the Barrett, Joyner, and Halenda (BJH) and Horvath−Kawazoe (HK) methods, as illustrated in Figure 1b. The pore-size distributions of BC and KBC were found to be mainly concentrated within 1−5 nm, with many mesopores and micropores, conforming to the results obtained from the N_2 adsorption/desorption curves. Moreover, more pores with diameters of 0−10 nm were detected on KBC, as verified in Figure 1b, demonstrating the function of high-temperature KOH activation on forming pore structures.

Table 1 shows the distribution of the specific surface area and pore structure of BC and KBC. Both BC and KBC mainly consist of micropores, the values for total surface area and total volume of KBC were obtained using the BET, and Langmuir approaches are much larger than those of BC, which is consistent with other findings. Previous studies have shown that microporous activated carbon is produced when chemical activation is performed with excess alkali (e.g., NaOH and KOH). Under a high temperature, KOH was transformed into K_2O and H_2O, and thereinto, fragile C could react with H_2O to produce H_2 and CO, thus inducing C loss and production of pore structures. K_2O could catalyze C reacting with H_2O, which aggravated C loss and production of pore structures. The increase in micropores may ultimately lead to pore

https://doi.org/10.1021/acsomega.2c04033
ACS Omega 2022, 7, 30543−30553

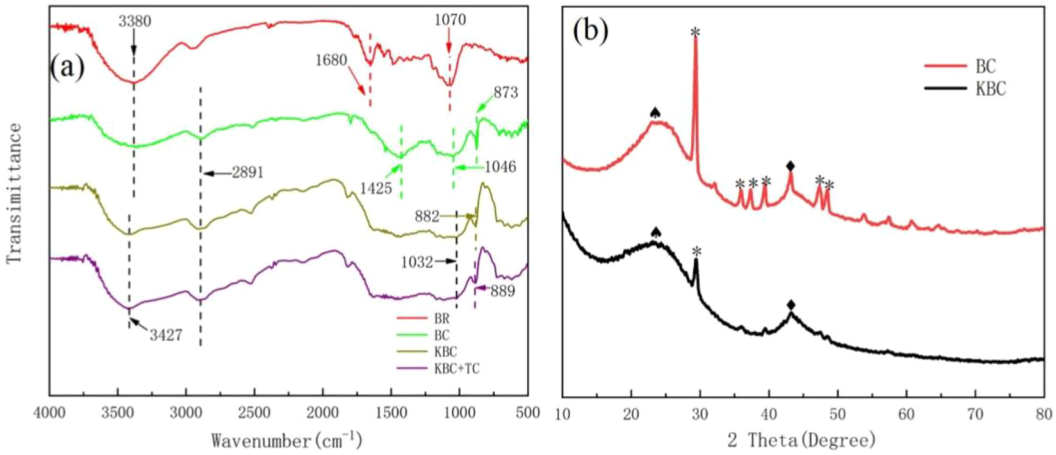

Figure 3. FTIR spectra of BR, BC, KBC, and KBC + TC (a) and the XRD patterns of BC and KBC (b).

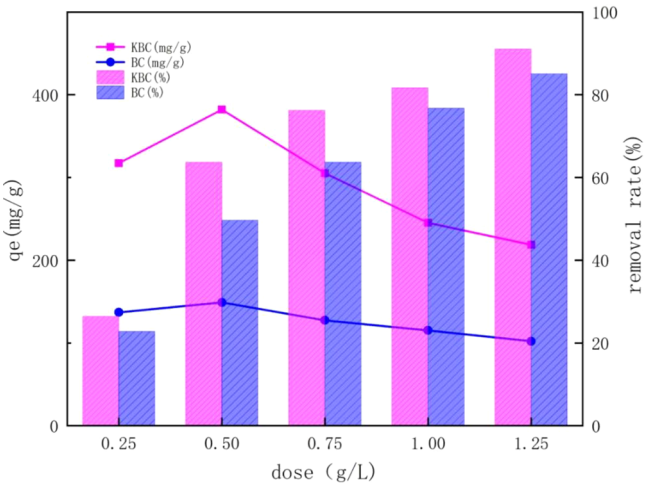

Figure 4. Impact of BC and KBC adsorbent dosage on removal efficiency and adsorption capacity of TC.

collapse and the formation of more mesopores and macropores.[31] Thus, the addition of KOH can promote the progress of microporous and mesoporous structures.

3.1.2. SEM and EDS. The surface morphologies of BR, BC, and KBC were studied with the use of SEM, and their elemental distribution was determined by EDS using the same instrument. The results are shown in Figure 2a–f and Table 2. Upon high-temperature pyrolysis, obvious porous structures could be detected on BC and KBC (Figure 2c–f. The EDS analyses of BR, BC, and KBC are shown in Table 2. C and O are the main elements, and also there is a small amount of N and Ca elements. Furthermore, the analyses demonstrated an increased C content and decreased O content on BC and KBC, upon high-temperature pyrolysis, which could result from the loss of O-including functional groups and water during pyrolysis.[32]

3.1.3. FTIR. Figure 3a illustrates the FT-IR spectra of BR, BC, and KBC. The broad peak near 3380 cm^{-1} originating from O–H stretching of the lignin, cellulose, and hemicellulose content of BR[33] was decreased on BC and KBC, which could be ascribed to the dehydrogenation and dehydration effect of high-temperature treatment. Meanwhile, upon high-temperature pyrolysis, weak intensity occurred on C–H stretching of 2891 cm^{-1} in the hemicellulose backbone[34] and carbonyl groups stretching of 1680 cm^{-1} in hemicellulose, which indicated the high temperature and KOH activation process decomposed part of the hemicellulose in BR.[35] Compared to BC, KOH activation decreased the intensity of C–C at 1425 cm^{-1}, and C–O at 1046 cm^{-1}, which could be ascribed to the reaction between K_2O and C under high temperature.

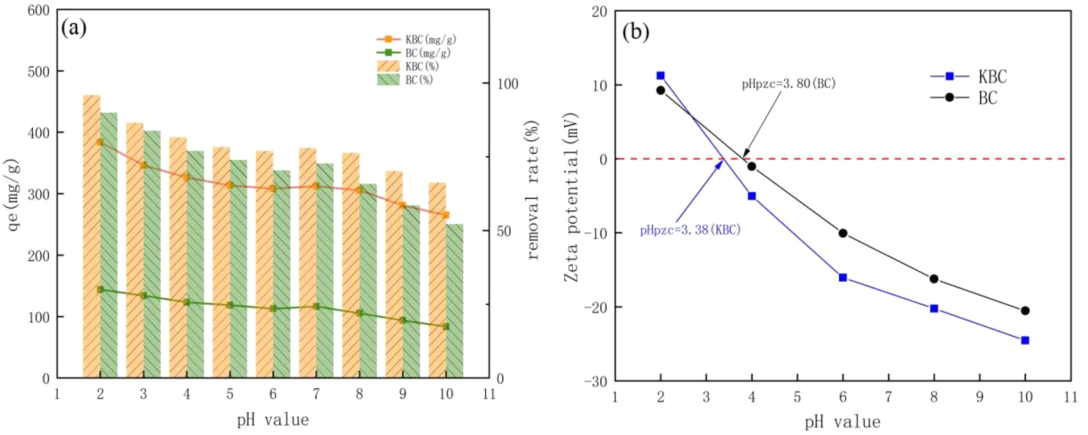

Figure 5. (a) Impact of solution pH on the adsorption of TC on BC and KBC, and (b) the variation of zeta potential of BC and KBC with solution pH.

https://doi.org/10.1021/acsomega.2c04033
ACS Omega 2022, 7, 30543–30553

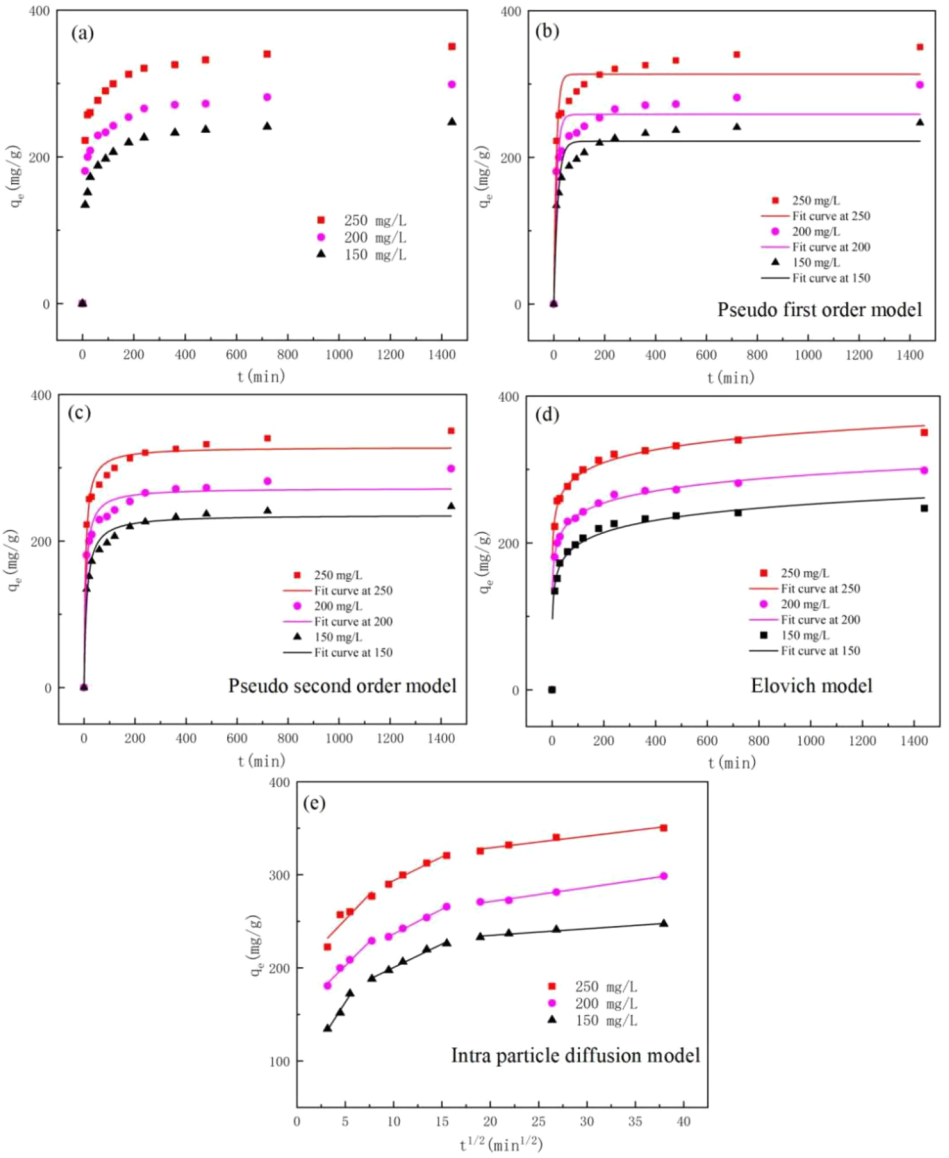

Figure 6. (a) Influence of contact time on TC adsorption of KBC and model fits to the experimental data: pseudo-first-order (b), pseudo-second-order (c), Elovich (d), and intraparticle diffusion (e).

Table 3. Extracted Kinetic Parameters of TC Adsorption on KBC

initial TC concentration C_0 (mg/L)	150	200	250
q_{exp} (mg/g)	247.11	298.70	350.30
pseudo-first-order			
q_{cal} (mg/g)	221.96	258.59	313.32
k_1 (min^{-1})	0.0631	0.0873	0.0984
R^2	0.913	0.909	0.931
pseudo-second-order			
q_{cal} (mg/g)	235.75	272.21	328.16
k_2 ($g \cdot min^{-1} \cdot mg^{-1}$)	4.08×10^{-4}	5.17×10^{-4}	5.07×10^{-4}
R^2	0.975	0.962	0.976
Elovich			
α ($g \cdot min^{-1} \cdot mg^{-1}$)	87.69	129.07	174.62
β (g/mg)	0.0418	0.0422	0.0393
R^2	0.976	0.991	0.979

However, although the number of functional groups of KBC was reduced, some organic functional groups were retained on the surface.[36]

3.1.4. XRD. Figure 3b presents the XRD patterns of BC and KBC. The distinct broad diffraction peak at 23.69° in both patterns indicates the presence of graphite-like structures (amorphous carbon) in both biochars, while the characteristic diffraction peak at 43.16° indicates the formation of crystalline graphitic structures.[37] The intensity of the latter diffraction peak is weaker in KBC than in BC, indicating that BC is slightly more graphitized than KBC, which may be the result of the destruction of some functional groups by KOH. The characteristic peaks at 29.34°, 35.95°, 37.34°, 39.42°, 47.34°, and 48.47° seen in the BC pattern correspond to $CaCO_3$ crystallites. After modification by high-temperature KOH and acid washing, most of these peaks disappeared, which indicated that $CaCO_3$ was removed.

3.2. Impact of Adsorbent Dosage. As shown in an adsorption system, the adsorbent dosage plays a vital role determining the adsorbent-adsorbent equilibrium. Figure 4

https://doi.org/10.1021/acsomega.2c04033
ACS Omega 2022, 7, 30543−30553

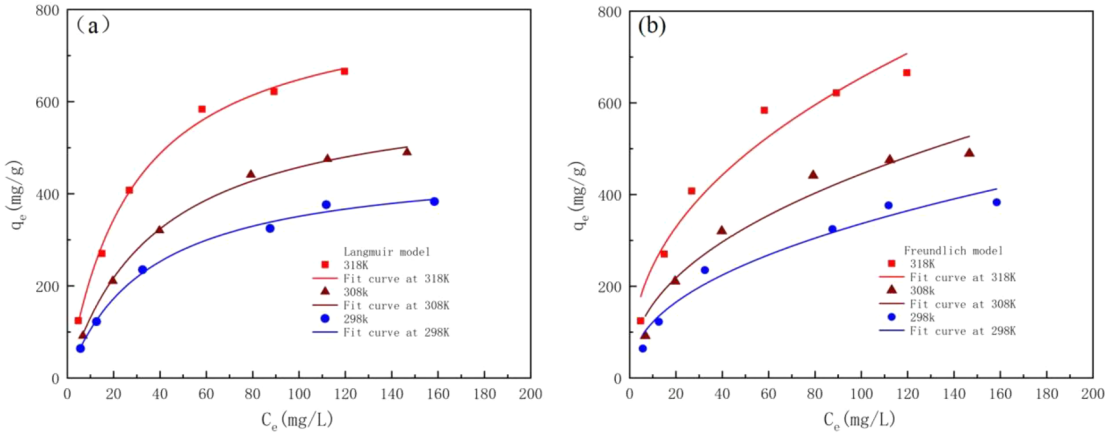

Figure 7. Langmuir (a) and Freundlich (b) isotherm model fits for TC adsorption of KBC.

Table 4. Extracted Fitting Parameters of the Langmuir and Freundlich Isotherm Models of TC on KBC

		Langmuir model				Freundlich model		
sample	temperature (K)	q_m (mg/g)	K_L (L/mg)	K (dimensionless)	R^2	K_F ($mg^{1-1/n}·g^{-1}·L^{-1/n}$)	$1/n$	R^2
KBC	298	473.66	0.0286	705602.6	0.992	43.99	0.4418	0.952
	308	631.86	0.0263	648858.3	0.996	57.94	0.4426	0.946
	318	830.78	0.0354	873368.3	0.994	91.35	0.4277	0.944

Table 5. Comparison of the TC Adsorption Capacities of KBC as well as Other Biomass-Based Adsorbents Reported

adsorbent	adsorption conditions	Q_{max} (mg/g)	ref
wheat straw derived biochar	45 °C	584.19	29
Eucommia ulmoides lignin-based biochar	55 °C, pH 6	1163	52
magnetic sludge biochar	0.2 g/L, 24 h, 35 °C, pH 6	145	48
agricultural biochar	5 g/L, 6 h, 25 °C, pH 7	9.45	47
rice straw derived biochar	1.2 g/L, 1 h, 25 °C	98.33	53
leaf-derived biochar	0.1 g/L, 5 days, 20 °C, pH 6	361	42
manganese dioxide modified biochar	0.8 g/L, 3 days, 35 °C, pH 3	131.49	54
reed-based biochar	24 h, 40 °C, pH 6	173.61	36
alfalfa-derived biochar	0.1 g/L, 5 days, 20 °C, pH 5	302.37	44

presents the impact of varying the dosage of BC and KBC on TC removal efficiency as well as adsorption capacity. Although the adsorption capacity of BC for tetracycline was limited, the removal efficiency progressively enhanced with increasing adsorbent dosage. At any given dosage, KBC had a higher removal efficiency and larger adsorption capacity in comparison with BC, indicating that KOH activation could obviously improve the TC adsorption performance of the adsorbent. With the dosage being enhanced from 0.25 g/L to 1.25 g/L, the removal efficiency of TC was initially enhanced and subsequently lowered. The initial increase could result from the increase in functional groups and effective contact area with increasing dosage, while the decrease at high dosage was due to the decrease in the effective contact surface of TC because of the overlapping of active sites. The highest adsorption of TC was achieved based on a KBC dosage of 0.5 g/L. For subsequent experiments, this level was maintained.

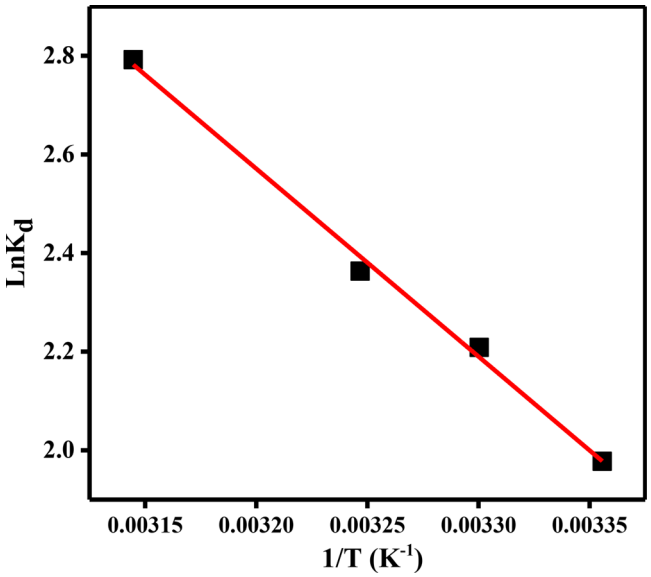

Figure 8. Thermodynamics of the adsorption of TC on KBC.

Table 6. Extracted Adsorption Thermodynamic Parameters for TC Adsorption on KBC

sample	T (K)	ΔG^0 (kJ·mol^{-1})	ΔH^0 (kJ·mol^{-1})	ΔS^0 (J·mol^{-1}·K^{-1})
KBC	298	−4.751	35.864	0.136
	303	−5.568		
	308	−6.114		
	318	−7.477		

3.3. Effect of pH. Figure 5a shows the impact of pH on the adsorption and removal behavior of BC and KBC. The adsorption of TC by KBC reached the maximum value of 380.75 mg/g at pH 2 and subsequently reduced slightly at higher pH. TC refers to an amphoteric molecule which has three pK_a values (3.3, 7.7 and 9.7) and, thereby, will occur in

https://doi.org/10.1021/acsomega.2c04033
ACS Omega 2022, 7, 30543−30553

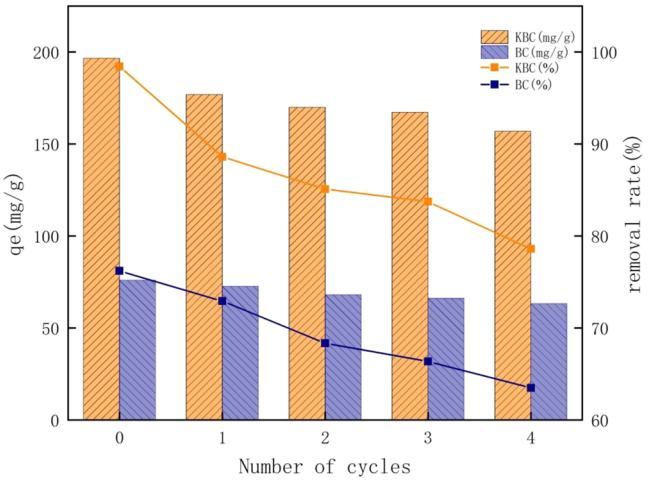

Figure 9. Regenerative properties of BC and KBC.

four different forms at different pHs: the cation $H4TC^+$ (pH < 3.4), the neutral molecule $H3TC^0$ (3.4 < pH < 7.6), the anion $H2TC^-$ (7.6 < pH < 9.7), and the double anion HTC (pH > 9.7).[38] In addition, the measured pH_{PZC} values of BC and KBC were 3.80 and 3.38, respectively. According to Figure 5b, the surface charge of the absorbents is therefore positively charged with solution pH < pH_{PZC} and negatively charged with solution pH > pH_{PZC}.[39] At 3.4 < pH < 7.6, $H3TC^0$ is the predominant form, KBC carries a slightly negative charge, and the electrostatic interaction and repulsion forces reach a minimum value, so there exists no significant change in the TC adsorption capacity of KBC at pH values of 4−7. At pH 2.3, TC molecules exist in cationic form, and the KBC surface also has a positive charge. As a result, the high TC adsorption capacity of KBC at this pH despite the electrostatic repulsion suggests other interactions between KBC and TC molecules, namely, strong hydrogen bonding and $\pi-\pi$ EDA interactions.[40] And the slight decrease in the TC adsorption capacity of KBC at pH > 7 can be attributed to both hydrogen bonding and $\pi-\pi$ EDA interaction forces being weakened under alkaline conditions, in addition to the presence of strong electrostatic repulsion between the negatively charged TC and BC surfaces. In addition, BC displays similar behavior, having the highest adsorption at pH 2−3, although, overall, the adsorption capacity of BC is much lower when compared with that of KBC.

3.4. Impact of Adsorption Time and the Adsorption Kinetics. Figure 6a shows the variation in TC adsorption on KBC with TC concentration. The trends are broadly TC concentration-independent, showing fast and then slow adsorption and eventually reaching the adsorption equilibrium. During the initial stage of adsorption, KBC is filled with a large number of adsorbable sites, and TC is rapidly adsorbed onto the surface of KBC; however, as the adsorption proceeds, the number of free adsorption sites progressively decreases with the surface adsorption reaching saturation; thereafter, the TC molecules migrate from the surface to the interior, and the rate of adsorption gradually decreases due to increasing diffusion resistance. When all of the adsorption sites of the biochar are occupied, the adsorption reaches equilibrium.[41]

The adsorption kinetics data were fitted using quasi primary, quasi secondary, and Elovich kinetic models. The relevant models are shown below:[42]

$$q_t = q_e[1 - e^{-k_1 t}] \tag{3}$$

$$q_t = \frac{k_2 q_e^2 t}{1 + k_2 q_e t} \tag{4}$$

$$q_t = \frac{1}{\beta} \ln(1 + \alpha\beta t) \tag{5}$$

where q_t refers to the adsorption amount at time t (mg/g), q_e indicates the adsorption amount at equilibrium (mg/g), k_1, k_2 are the pseudo-first-order and pseudo-second-order reaction rate constants, and α, β stand for the initial adsorption rate

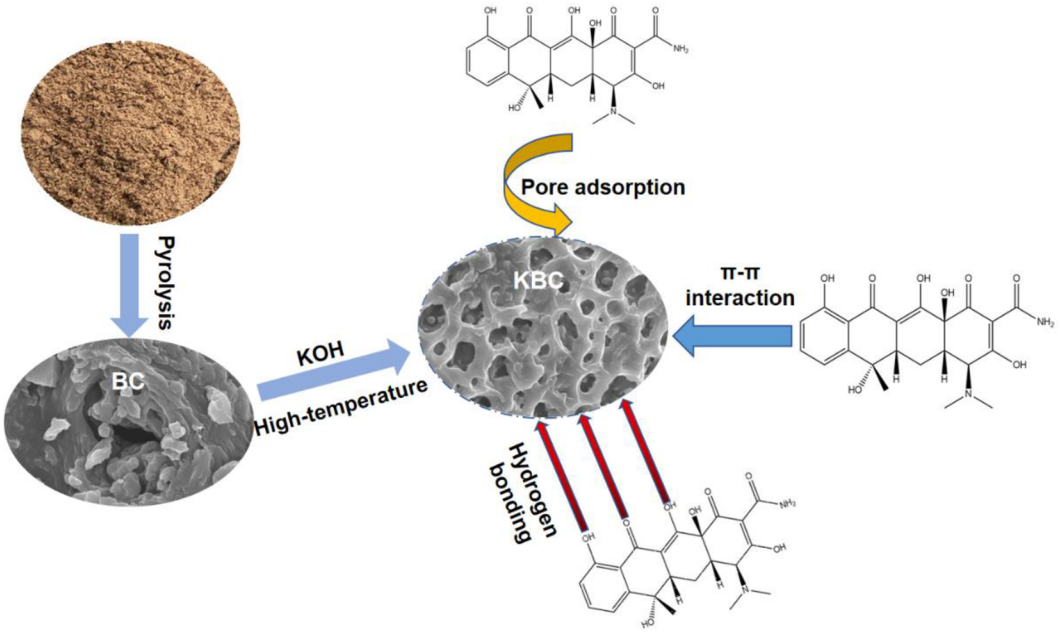

Figure 10. Schematic diagram of the combination of three mechanisms responsible for the adsorption of TC on KBC.

https://doi.org/10.1021/acsomega.2c04033
ACS Omega 2022, 7, 30543−30553

constants and parameters associated with the activation energy during the adsorption process, separately.

The fitted curves and extracted parameters of the three adsorption models are shown in Figure 6b−d and Table 3. For the purpose of assessing the fitting level of the adsorption model, the determination coefficient (R^2) could be adopted. As the initial TC concentration remained unchanged, a greater R^2 could be attained in pseudo-second-order and Elovich kinetic models, demonstrating they fit TC adsorption kinetics, which is consistent with the findings of former research studies.[43,44] Pseudo-second-order kinetics are consistent with adsorption via pore filling, covalent bond formation, and electron exchange, while the Elovich model supposes that the adsorbent surface can be energetically heterogeneous and that chemisorption interactions occur.[45] Therefore, the adsorption of TC by KBC proceeds via both electrostatic interactions.

The particle diffusion model was performed with the purpose of further exploring the TC adsorption mechanism of KBC. The equation for this model is[46]

$$q_t = k_{id} t^{1/2} + C_i \tag{6}$$

where k_{id} indicates the intraparticle diffusion rate constant ($mg \cdot g \cdot min^{-1/2}$), and C_i refers to the boundary layer constant.

Figure 6e shows the results of the fit. The curve consists of three linear elements, suggesting that the adsorption process is categorized into the following three stages: (1) an external diffusion stage, where TC is transferred to the surface of KBC through the water film; (2) an internal diffusion stage, where TC molecules enter the internal surface through the pores of KBC; and (3) an adsorption equilibrium stage, where the adsorption of TC by KBC reaches saturation. Since none of the linear curves crossed the origin, apart from intraparticle diffusion, other processes were possibly involved into TC adsorption.[47]

3.5. Impact of Initial TC Concentration and the Adsorption Isotherms. As Figure 7 displayed the adsorption capacity under different equilibrium concentration, the adsorbed amount of TC increased with its increased concentration in solution under an equilibrium state. With the further increase on TC equilibrium concentration than 100 mg/L, TC adsorption capacity was slightly increased, which could be ascribed to the saturation of adsorption sites on biochar. Langmuir and Freundlich isotherm was adopted for assessing the adsorption capacity of biochar on TC, as illustrated in Figure 7. Besides, Table 4 shows the extracted fitting parameters. Equations 7 and 8 show the Langmuir and Freundlich models, respectively:[48]

$$q_e = \frac{q_m K_L C_e}{1 + K_L C_e} \tag{7}$$

$$q_e = K_F C_e^{1/n} \tag{8}$$

where q_e denotes the adsorption capacity at equilibrium adsorption, C_e refers to the equilibrium concentration of TC, q_m is the maximum adsorption capacity (mg/g), n represents the heterogeneity factor, K_L suggests the Langmuir constant (L/mg), and K_F means the Freundlich constant (mg/g).

Adsorption capacity at equilibrium at first increased with enhancing the initial TC concentration—which may be caused by the enhancement in concentration leading to a corresponding increase in driving force[49]—before leveling off. The Langmuir model proved a better fit for the observed adsorption of KBC on TC, suggesting that the adsorption of KBC on TC is mostly monolayer adsorption.[50] Monolayer adsorption from the Langmuir model was positively associated with the specific surface areas and developed pore structure, and such a result could explain the high performance of KBC on TC adsorption, with the maximum adsorption of 830.78 mg/g at 318 k. It was also seen that the values of $1/n$ in the Freundlich model fit are less than 0.5, showing that KBC can easily adsorb TC.[51] It should also be noted here that KBC shows better TC adsorption than many other adsorbents described in the literature (Table 5).

3.6. Impact of Temperature and a Study of the Thermodynamics. The parameters of the thermodynamic processes involved in TC adsorption on KBC can be defined and calculated based on the subsequent equation.[55]

$$K_d = \frac{q_e}{C_e} \tag{9}$$

$$\ln K_d = \frac{\Delta S^0}{R} - \frac{\Delta H^0}{RT} \tag{10}$$

$$\Delta G^0 = \Delta H^0 - \Delta S^0 T \tag{11}$$

where K_d is the distribution coefficient, ΔG^0 refers to the change in Gibbs free energy ($kJ \cdot mol^{-1}$), ΔS^0 refers to the change in entropy ($J \cdot mol^{-1} \cdot K^{-1}$), ΔH^0 suggests the change in enthalpy ($kJ \cdot mol^{-1}$), the absolute temperature (K), and R represents the universal gas constant ($8.314 J \cdot mol^{-1} \cdot K^{-1}$).

Figure 8 shows the plot of ln K_d versus $1/T$. ΔH^0 and ΔS^0 are computed from the slope and intercept of the linear plot, allowing ΔG^0 to be calculated according to eq 11. The extracted parameters are shown in Table 6. On the basis of Table 6, ΔG^0 is below zero at all temperatures, suggesting that the adsorption process of KBC on TC is spontaneous. As ΔG^0 decreases with increasing temperatures, this suggests that heat enhances the spontaneity of the adsorption. It can also be seen that ΔH^0 is greater than zero, implying that the adsorption process can be an endothermic reaction. Apart from that, the positive ΔS^0 value is also favorable.

3.7. Recyclability of the Adsorbent. The regeneration performance of the prepared adsorbent was assessed using adsorption−desorption experiments across several cycles. Figure 9 shows the adsorption performance of the adsorbents across four adsorption cycles. With the increase of cycle times, the adsorption capacity of KBC for TC decreased from 196.67 mg/g to 156.99 mg/g, BC for TC decreased from 76.01 mg/g to 63.29 mg/g, which could be ascribed to the residual TC on biochar that could not be desorbed by NaOH and deionized water. TC adsorption capacity and removal rate remained high after four cycles, demonstrating the great regeneration performance of KBC on TC adsorption.

3.8. Adsorption Mechanism(s). Both the functional groups and the physical structure of the adsorbent surface generate obvious impacts on the adsorption of TC. The analysis of the impact of different pH values on TC adsorption by KBC demonstrated that the electrostatic effect was negligible, which indicates that TC adsorption does not proceed via an electrostatic effect. Instead, we propose that a combination of three alternative mechanisms is responsible for TC adsorption by KBC—the detailed mechanism of action is shown in Figure 10. The first contributing mechanism is pore adsorption—it has been reported[56] that carbonaceous materials with high specific surface area and high pore volume

https://doi.org/10.1021/acsomega.2c04033
ACS Omega 2022, 7, 30543−30553

stimulate the adsorption of organic matter because of their obvious pore filling effect. Thus, the carbonized, high-temperature KOH-activated KBC with its well-developed micro- and mesoporous structures and relatively high surface area could remove TC molecules by physical diffusion. The second contributing mechanism is hydrogen bonding. On the basis of the analysis of FTIR spectra, the 3427 cm^{-1} peak of KBC was enhanced after adsorption, and the position of the C−H peak at 882 cm^{-1} shifted, both of which are an indication of the removal of TC molecules by hydrogen bonding between KBC and functional groups in the TC molecules. The final contributing mechanism is the $\pi-\pi$EDA stacking interaction. The XRD analysis showed that KBC has a graphitized structure rich in π electrons, which may interact with the aromatic and amino structures in TC molecules by $\pi-\pi$ EDA.[57]

4. CONCLUSIONS

In the present study, *Caulis spatholobi* residue was used to prepare biochar. High-temperature KOH activation was conducted to improve biochar with more developed pore structures and greater specific surface area, which could be verified by BET analysis, SEM images, EDS elementary analysis, FTIR, and XRD. pH displayed a slight influence on tetracycline adsorption, which signified the slight influence of the existence of tetracycline and the charge potential of biochar. Accordingly, TC adsorption on biochar possibly originated from pore filling, hydrogen bonding, and $\pi-\pi$ EDA stacking interaction. TC adsorption kinetics was better fitted by pseudo-second-order and Elovich kinetic models, demonstrating the involvement of chemisorption and physisorption in TC adsorption. Relative to the Freundlich isotherm model, the Langmuir isotherm model better matched TC adsorption, demonstrating the relation between TC adsorption and the specific surface areas of biochar, as well as the developed pore structure. Besides, the maximum adsorption capacity of KBC on TC was 830.78 mg/g at 318 K. The optimal pH for TC adsorption was 2. As displayed by thermodynamic analysis, TC adsorption on KBC was an endothermic reaction process. KBC also showed good thermal stability and regeneration performance.

AUTHOR INFORMATION

Corresponding Author

Zheng Fan − *Membrane Separation and Water Treatment Center, Zhejiang University of Technology, State Key Lab Breeding Base of Green Chemical Synthesis Technology, Hangzhou 310014, China;* orcid.org/0000-0003-2509-1829; Email: fanzh@zjut.edu.cn

Authors

Jie Fang − *School of Chemical Engineering, Zhejiang University of Technology, Hangzhou 310014, China*

Guoliang Zhang − *Membrane Separation and Water Treatment Center, Zhejiang University of Technology, State Key Lab Breeding Base of Green Chemical Synthesis Technology, Hangzhou 310014, China;* orcid.org/0000-0002-7371-3349

Lei Qin − *Membrane Separation and Water Treatment Center, Zhejiang University of Technology, State Key Lab Breeding Base of Green Chemical Synthesis Technology, Hangzhou 310014, China;* orcid.org/0000-0001-6842-4924

Zhenzhen Fang − *School of Chemical Engineering, Zhejiang University of Technology, Hangzhou 310014, China*

Laiyun Jin − *School of Chemical Engineering, Zhejiang University of Technology, Hangzhou 310014, China*

Complete contact information is available at: https://pubs.acs.org/10.1021/acsomega.2c04033

Notes

The authors declare no competing financial interest.

ACKNOWLEDGMENTS

We appreciate the financial assistance from the National Natural Science Foundation of China (Grant No. 21736009), the Zhejiang Public Welfare Research Project (Grant No. LGF19B070005), the Basic Public Welfare Research Program of Zhejiang Province (Grant No. 2021C03169), and the Scientific Research Foundation of Zhejiang University of Technology (201910337011).

ABBREVIATIONS

C_0 and C_t	initial TC concentration and concentration (mg/L) of TC solution at a time t
V	the initial volume of the solution (mL)
W	mass of adsorbent (g)
BR	*Caulis spatholobi* residue
TC	tetracycline
BC	biochar derived from *Caulis spatholobi* residue
KBC	*Caulis spatholobi* residue biochar with potassium hydroxide as an activator
k_1, k_2	pseudo-first-order and pseudo-second-order rate constants
k_{id}	intraparticle diffusion rate constant
C_i	boundary layer constant
K_F and n	Freundlich constants
K_L	Langmuir constant
q_e	adsorption capacity of adsorbent (mg/g)
q_m	the maximum adsorption capacity of adsorbents (mg/g)
q_t	quantity adsorbed at time t
E_q	TC removal rate
R^2	determination coefficient
$\pi-\pi$ EDA stacking interaction	a noncovalent interaction

REFERENCES

(1) Chen, K.; Zhou, J. L. Occurrence and Behavior of Antibiotics in Water and Sediments from the Huangpu River, Shanghai, China. *Chemosphere* **2014**, *95*, 604−612.

(2) Xu, Z.; Li, T.; Bi, J.; Wang, C. Spatiotemporal Heterogeneity of Antibiotic Pollution and Ecological Risk Assessment in Taihu Lake Basin, China. *Sci. Total Environ.* **2018**, *643* (163), 12−20.

(3) Praveena, S. M.; Shaifuddin, S. N. M.; Sukiman, S.; Nasir, F. A. M.; Hanafi, Z.; Kamarudin, N.; Ismail, T. H. T.; Aris, A. Z. Pharmaceuticals Residues in Selected Tropical Surface Water Bodies from Selangor (Malaysia): Occurrence and Potential Risk Assessments. *Sci. Total Environ.* **2018**, *642*, 230−240.

(4) Balakrishna, K.; Rath, A.; Praveenkumarreddy, Y.; Guruge, K. S.; Subedi, B. A Review of the Occurrence of Pharmaceuticals and Personal Care Products in Indian Water Bodies. *Ecotoxicol. Environ. Saf.* **2017**, *137*, 113−120.
(5) Chen, H.; Jing, L.; Teng, Y.; Wang, J. Characterization of Antibiotics in a Large-Scale River System of China: Occurrence Pattern, Spatiotemporal Distribution and Environmental Risks. *Sci. Total Environ.* **2018**, *618*, 409−418.
(6) Scaria, J.; Anupama, K. V.; Nidheesh, P. V. Science of the Total Environment Tetracyclines in the Environment : An Overview on the Occurrence, Fate, Toxicity, Detection, Removal Methods, and Sludge Management. *Sci. Total Environ.* **2021**, *771*, 145291.
(7) Gossen, M.; Bujard, H. Tight Control of Gene Expression in Mammalian Cells by Tetracycline-Responsive Promoters. *Proc. Natl. Acad. Sci. U. S. A.* **1992**, *89* (12), 5547−5551.
(8) Gothwal, R.; Shashidhar, T. Antibiotic Pollution in the Environment: A Review. *Clean - Soil, Air, Water* **2015**, *43* (4), 479−489.
(9) Ahmed, M. B.; Zhou, J. L.; Ngo, H. H.; Guo, W.; Thomaidis, N. S.; Xu, J. Progress in the Biological and Chemical Treatment Technologies for Emerging Contaminant Removal from Wastewater: A Critical Review. *J. Hazard. Mater.* **2017**, *323*, 274−298.
(10) Wang, J.; Zhuan, R. Degradation of Antibiotics by Advanced Oxidation Processes: An Overview. *Sci. Total Environ.* **2020**, *701*, 135023.
(11) Ma, J.; Xiong, Y.; Dai, X.; Yu, F. Coadsorption Behavior and Mechanism of Ciprofloxacin and Cu(II) on Graphene Hydrogel Wetted Surface. *Chem. Eng. J.* **2020**, *380*, 122387.
(12) Song, J.; Wu, X.; Zhang, M.; Liu, C.; Yu, J.; Sun, G.; Si, Y.; Ding, B. Highly Flexible, Core-Shell Heterostructured, and Visible-Light-Driven Titania-Based Nanofibrous Membranes for Antibiotic Removal and E. Coil Inactivation. *Chem. Eng. J.* **2020**, *379*, 122269.
(13) Hayati, F.; Isari, A. A.; Anvaripour, B.; Fattahi, M.; Kakavandi, B. Ultrasound-Assisted Photocatalytic Degradation of Sulfadiazine Using MgO@CNT Heterojunction Composite: Effective Factors, Pathway and Biodegradability Studies. *Chem. Eng. J.* **2020**, *381*, 122636.
(14) Naeem, M. A.; Imran, M.; Amjad, M.; Abbas, G.; Tahir, M.; Murtaza, B.; Zakir, A.; Shahid, M.; Bulgariu, L.; Ahmad, I. Batch and Column Scale Removal of Cadmium from Water Using Raw and Acid Activated Wheat. *Water* **2019**, *11*, 1438.
(15) Lucaci, A. R.; Bulgariu, D.; Ahmad, I.; Lisa, G.; Mocanu, A. M.; Bulgariu, L. Potential Use of Biochar from Various Waste Biomass as Biosorbent in Co(II) Removal Processes. *Potential Use of Biochar from Various Waste Biomass as Biosorbent in Co (II) Removal Processes.* **2019**, *11*, 1565.
(16) Wu, L.; Li, B.; Liu, M. Influence of Aromatic Structure and Substitution of Carboxyl Groups of Aromatic Acids on Their Sorption to Biochars. *Chemosphere* **2018**, *210*, 239−246.
(17) Zhu, X.; Li, C.; Li, J.; Xie, B.; Lü, J.; Li, Y. Thermal Treatment of Biochar in the Air/Nitrogen Atmosphere for Developed Mesoporosity and Enhanced Adsorption to Tetracycline. *Bioresour. Technol.* **2018**, *263* (May), 475−482.
(18) Dai, Y.; Zhang, N.; Xing, C.; Cui, Q.; Sun, Q. The Adsorption, Regeneration and Engineering Applications of Biochar for Removal Organic Pollutants: A Review. *Chemosphere* **2019**, *223*, 12−27.
(19) Wang, Y. X.; Ngo, H. H.; Guo, W. S. Preparation of a Specific Bamboo Based Activated Carbon and Its Application for Ciprofloxacin Removal. *Sci. Total Environ.* **2015**, *533*, 32−39.
(20) Wang, B.; Li, Y.-n.; Wang, L. Metal-Free Activation of Persulfates by Corn Stalk Biochar for the Degradation of Antibiotic Norfloxacin: Activation Factors and Degradation Mechanism. *Chemosphere* **2019**, *237*, 124454.
(21) Dassharma, D.; Samanta, S.; Dharun Nithish Kumar, S.; Halder, G. A Mechanistic Insight into Enrofloxacin Sorptive Affinity of Chemically Activated Carbon Engineered from Green Coconut Shell. *J. Environ. Chem. Eng.* **2020**, *8* (5), 104140.
(22) Zhou, Y.; Selvam, A.; Wong, J. W. C. Bioresource Technology Chinese Medicinal Herbal Residues as a Bulking Agent for Food Waste Composting. *Bioresour. Technol.* **2018**, *249*, 182−188.
(23) Wang, H.; Lou, X.; Hu, Q.; Sun, T. Adsorption of Antibiotics from Water by Using Chinese Herbal Medicine Residues Derived Biochar : Preparation and Properties Studies. *J. Mol. Liquids* **2021**, *325*, 2−10.
(24) Cha, J. S.; Park, S. H.; Jung, S. C.; Ryu, C.; Jeon, J. K.; Shin, M. C.; Park, Y. K. Production and Utilization of Biochar: A Review. *J. Ind. Eng. Chem.* **2016**, *40*, 1−15.
(25) Sun, K.; Kang, M.; Zhang, Z.; Jin, J.; Wang, Z.; Pan, Z.; Xu, D.; Wu, F.; Xing, B. Impact of Deashing Treatment on Biochar Structural Properties and Potential Sorption Mechanisms of Phenanthrene. *Environ. Sci. Technol.* **2013**, *47*, 11473.
(26) Huang, S. Y.; Qin, J. X. Progress of the pharmacological effect of Caulis spatholobi. *Lishizhen Medicine and Materia Medica Res.* **2014**, *25* (1), 180−183.
(27) Fan, Z.; Zhang, Z.; Zhang, G.; Qin, L.; Fang, J.; Tao, P. Phosphoric Acid/$FeCl_3$ Converting Waste Mangosteen Peels into Bio-Carbon Adsorbents for Methylene Blue Removal. *Int. J. Environ. Sci. Technol.* **2022**, 0123456789.
(28) Choi, Y. K.; Choi, T. R.; Gurav, R.; Bhatia, S. K.; Park, Y. L.; Kim, H. J.; Kan, E.; Yang, Y. H. Adsorption Behavior of Tetracycline onto Spirulina Sp. (Microalgae)-Derived Biochars Produced at Different Temperatures. *Sci. Total Environ.* **2020**, *710*, 136282.
(29) Xu, J.; Zhang, Y.; Li, B.; Fan, S.; Xu, H.; Guan, D. X. Improved Adsorption Properties of Tetracycline on KOH/KMnO4Modified Biochar Derived from Wheat Straw. *Chemosphere* **2022**, *296*, 133981.
(30) Tran, T. H.; Le, A. H.; Pham, T. H.; Nguyen, D. T.; Chang, S. W.; Chung, W. J.; Nguyen, D. D. Adsorption Isotherms and Kinetic Modeling of Methylene Blue Dye onto a Carbonaceous Hydrochar Adsorbent Derived from Coffee Husk Waste. *Sci. Total Environ.* **2020**, *725*, 138325.
(31) Martins, A. C.; Pezoti, O.; Cazetta, A. L.; Bedin, K. C.; Yamazaki, D. A. S.; Bandoch, G. F. G.; Asefa, T.; Visentainer, J. V.; Almeida, V. C. Removal of Tetracycline by NaOH-Activated Carbon Produced from Macadamia Nut Shells: Kinetic and Equilibrium Studies. *Chem. Eng. J.* **2015**, *260*, 291−299.
(32) Choi, Y. K.; Kan, E. Effects of Pyrolysis Temperature on the Physicochemical Properties of Alfalfa-Derived Biochar for the Adsorption of Bisphenol A and Sulfamethoxazole in Water. *Chemosphere* **2019**, *218*, 741−748.
(33) Wei, L.; Liang, S.; Guho, N. M.; Hanson, A. J.; Smith, M. W.; Garcia-Perez, M.; McDonald, A. G. Production and Characterization of Bio-Oil and Biochar from the Pyrolysis of Residual Bacterial Biomass from a Polyhydroxyalkanoate Production Process. *J. Anal. Appl. Pyrolysis* **2015**, *115*, 268−278.
(34) Wang, H.; Sun, Y.; Zhu, T.; Wang, W.; Deng, H. Adsorption of Acetaldehyde onto Carbide-Derived Carbon Modified by Oxidation. *Chem. Eng. J.* **2015**, *273*, 580−587.
(35) Baytar, O.; Sahin, Ö.; Saka, C. Sequential Application of Microwave and Conventional Heating Methods for Preparation of Activated Carbon from Biomass and Its Methylene Blue Adsorption. *Appl. Therm. Eng.* **2018**, *138*, 542−551.
(36) Zhao, C.; Ma, J.; Li, Z.; Xia, H.; Liu, H.; Yang, Y. Highly Enhanced Adsorption Performance of Tetracycline Antibiotics on KOH-Activated Biochar Derived from Reed Plants. *RSC Adv.* **2020**, *10* (9), 5066−5076.
(37) Yan, L.; Liu, Y.; Zhang, Y.; Liu, S.; Wang, C.; Chen, W.; Liu, C.; Chen, Z.; Zhang, Y. ZnCl2Modified Biochar Derived from Aerobic Granular Sludge for Developed Microporosity and Enhanced Adsorption to Tetracycline. *Bioresour. Technol.* **2020**, *297*, 122381.
(38) Jang, H. M.; Yoo, S.; Choi, Y. K.; Park, S.; Kan, E. Adsorption Isotherm, Kinetic Modeling and Mechanism of Tetracycline on Pinus Taeda-Derived Activated Biochar. *Bioresour. Technol.* **2018**, *259*, 24−31.
(39) Zeng, S.; Choi, Y. K.; Kan, E. Iron-Activated Bermudagrass-Derived Biochar for Adsorption of Aqueous Sulfamethoxazole: Effects

https://doi.org/10.1021/acsomega.2c04033
ACS Omega 2022, 7, 30543−30553

of Iron Impregnation Ratio on Biochar Properties, Adsorption, and Regeneration. *Sci. Total Environ.* **2021**, *750*, 141691.
(40) Xu, Z.; Xiang, Y.; Zhou, H.; Yang, J.; He, Y.; Zhu, Z.; Zhou, Y. Manganese Ferrite Modified Biochar from Vinasse for Enhanced Adsorption of Levofloxacin: Effects and Mechanisms. *Environ. Pollut.* **2021**, *272*, 115968.
(41) Zhang, P.; Li, Y.; Cao, Y.; Han, L. Characteristics of Tetracycline Adsorption by Cow Manure Biochar Prepared at Different Pyrolysis Temperatures. *Bioresour. Technol.* **2019**, *285* (April), 121348.
(42) Kim, J. E.; Bhatia, S. K.; Song, H. J.; Yoo, E.; Jeon, H. J.; Yoon, J. Y.; Yang, Y.; Gurav, R.; Yang, Y. H.; Kim, H. J.; Choi, Y. K. Adsorptive Removal of Tetracycline from Aqueous Solution by Maple Leaf-Derived Biochar. *Bioresour. Technol.* **2020**, *306* (March), 123092.
(43) Zhou, Y.; Liu, X.; Xiang, Y.; Wang, P.; Zhang, J.; Zhang, F.; Wei, J.; Luo, L.; Lei, M.; Tang, L. Modification of Biochar Derived from Sawdust and Its Application in Removal of Tetracycline and Copper from Aqueous Solution: Adsorption Mechanism and Modelling. *Bioresour. Technol.* **2017**, *245* (July), 266−273.
(44) Jang, H. M.; Kan, E. Engineered Biochar from Agricultural Waste for Removal of Tetracycline in Water. *Bioresour. Technol.* **2019**, *284* (March), 437−447.
(45) Zhu, X.; Liu, Y.; Qian, F.; Zhou, C.; Zhang, S.; Chen, J. Preparation of Magnetic Porous Carbon from Waste Hydrochar by Simultaneous Activation and Magnetization for Tetracycline Removal. *Bioresour. Technol.* **2014**, *154*, 209−214.
(46) Fan, X.; Qian, Z.; Liu, J.; Geng, N.; Hou, J.; Li, D. Investigation on the Adsorption of Antibiotics from Water by Metal Loaded Sewage Sludge Biochar. *Water Sci. Technol.* **2021**, *83* (3), 739−750.
(47) Hoslett, J.; Ghazal, H.; Katsou, E.; Jouhara, H. The Removal of Tetracycline from Water Using Biochar Produced from Agricultural Discarded Material. *Sci. Total Environ.* **2021**, *751*, 141755.
(48) Ma, Y.; Li, M.; Li, P.; Yang, L.; Wu, L.; Gao, F.; Qi, X.; Zhang, Z. Hydrothermal Synthesis of Magnetic Sludge Biochar for Tetracycline and Ciprofloxacin Adsorptive Removal. *Bioresour. Technol.* **2021**, *319*, 124199.
(49) Liu, H.; Xu, G.; Li, G. The Characteristics of Pharmaceutical Sludge-Derived Biochar and Its Application for the Adsorption of Tetracycline. *Sci. Total Environ.* **2020**, *747*, 141492.
(50) Zhang, X.; Zhang, Y.; Ngo, H. H.; Guo, W.; Wen, H.; Zhang, D.; Li, C.; Qi, L. Characterization and Sulfonamide Antibiotics Adsorption Capacity of Spent Coffee Grounds Based Biochar and Hydrochar. *Sci. Total Environ.* **2020**, *716*, 137015.
(51) Zeng, S.; Kan, E. Chemical Activation of Forage Grass-Derived Biochar for Treatment of Aqueous Antibiotic Sulfamethoxazole. *ACS Omega* **2020**, *5* (23), 13793−13801.
(52) Chen, Y.; Liu, J.; Zeng, Q.; Liang, Z.; Ye, X.; Lv, Y.; Liu, M. Preparation of Eucommia Ulmoides Lignin-Based High-Performance Biochar Containing Sulfonic Group: Synergistic Pyrolysis Mechanism and Tetracycline Hydrochloride Adsorption. *Bioresour. Technol.* **2021**, *329* (2), 124856.
(53) Dai, J.; Meng, X.; Zhang, Y.; Huang, Y. Effects of Modification and Magnetization of Rice Straw Derived Biochar on Adsorption of Tetracycline from Water. *Bioresour. Technol.* **2020**, *311* (April), 123455.
(54) Shen, Q.; Wang, Z.; Yu, Q.; Cheng, Y.; Liu, Z.; Zhang, T.; Zhou, S. Removal of Tetracycline from an Aqueous Solution Using Manganese Dioxide Modified Biochar Derived from Chinese Herbal Medicine Residues. *Environ. Res.* **2020**, *183*, 109195.
(55) Sheng, X.; Wang, J.; Cui, Q.; Zhang, W.; Zhu, X. A Feasible Biochar Derived from Biogas Residue and Its Application in the Efficient Adsorption of Tetracycline from an Aqueous Solution. *Environ. Res.* **2022**, *207*, 112175.
(56) Zhu, X.; Liu, Y.; Zhou, C.; Luo, G.; Zhang, S.; Chen, J. A Novel Porous Carbon Derived from Hydrothermal Carbon for Efficient Adsorption of Tetracycline. *Carbon N. Y.* **2014**, *77*, 627−636.
(57) Tran, H. N.; Tomul, F.; Thi Hoang Ha, N.; Nguyen, D. T.; Lima, E. C.; Le, G. T.; Chang, C. T.; Masindi, V.; Woo, S. H. Innovative Spherical Biochar for Pharmaceutical Removal from Water: Insight into Adsorption Mechanism. *J. Hazard. Mater.* **2020**, *394*, 122255.

https://doi.org/10.1021/acsomega.2c04033
ACS Omega 2022, 7, 30543−30553